

An experimental investigation of the intrinsic convection in a sedimenting suspension

Yannick Peysson and Élisabeth Guazzelli

Laboratoire de Physique et Mécanique des Milieux Hétérogènes, URA 857 au CNRS, ESPCI,
10 rue Vauquelin, 75231 Paris Cedex 05, France

(Received 21 May 1997; accepted 22 August 1997)

The sedimentation of spheres in a Newtonian fluid is experimentally studied under creeping flow conditions. The mean particle settling velocity and the particle velocity fluctuations are measured across the width of the sedimentation cell. We show that there can be a global intrinsic convection of the suspension superimposed on the settling motion of the particles. Unlike the predictions of the dilute theories of intrinsic convection, this effect is found to be small and even to disappear with increasing concentrations. We also find that there is an ordering of the suspension near the wall, which may be responsible for the observed small magnitude of the convection. © 1998 American Institute of Physics. [S1070-6631(98)00801-0]

I. INTRODUCTION

Although it can be considered, in principle, as one of the simplest examples of suspension flow, the problem of particle sedimentation in a viscous Newtonian fluid is complicated by the dominance of long-range multibody hydrodynamic interactions. In particular, the difficulty of determining the effect of concentration on the sedimentation velocity of a suspension of spheres derives from the slow decay of the perturbation of the fluid flow caused by a particle.

Batchelor¹ was the first to compute, to a first order in particle volume fraction, ϕ , the particle sedimentation velocity relative to the average volume velocity, i.e., relative to the suspension velocity, in the case of a dilute, random and infinite suspension in which pair interactions dominate. He showed that this relative velocity is hindered by particle interactions in particular through the fluid back flow.

Later, Mazur and his co-workers²⁻⁴ addressed the question of the dependence of the sedimentation velocity on the shape of the container. They found that the relative sedimentation velocity is shape independent and has, indeed, the value found by Batchelor¹ but that there exists a convection of the suspension in which the fluid and the particles move together. The amplitude of this convection is $O(V_S\phi)$, where V_S is the sedimentation velocity of an isolated sphere, and therefore is comparable to the first correction to the sedimentation velocity found by Batchelor.¹

This convection phenomenon which occurs in the sedimentation of an homogeneous suspension has been called *intrinsic convection*. Nozières⁵ showed that it could be understood, on a macroscopic level, as a consequence of the local coupling between the relative velocity field and the average volume velocity field. The phenomenological equations of Nozières were derived by Noetinger⁶ by using the method of Mazur and van Saarloos to compute the many-sphere hydrodynamic interactions.⁷

More recently, Bruneau *et al.*⁸ calculated this convection by using a simple model in which the particles were represented by an excluded volume and by point forces at their centers. In this approximation, the deficit in point forces near the wall produces a deficit in suspension density near the

wall. This buoyant particle-depleted layer located at one particle radius from the wall drives an upward flow near the wall. The circulation is completed by a downward return flow in the center. Moreover, when expressed with a boundary layer formulation, the model shows that the intrinsic convection reduces to a Poiseuille flow with a slip velocity at the wall, $w_* = 9V_S\phi/4$. The predictions of this simple point-force suspension model are in good agreement with those of Geigenmüller and Mazur³ which have a uniform distribution of point forces distributed over the surface of the particles.

An attempt has been recently made to incorporate the effect of particle-wall interactions in a dilute sedimenting suspension.⁹ The slip velocity at the wall was found to be increased and therefore the intrinsic convection to be intensified. Conversely, when the effect of particle concentration was included in the point-force suspension model, i.e., in a model without hydrodynamic interactions, by assuming an equilibrium distribution of hard spheres in the near wall region and using a Percus-Yevick approximation for this distribution, the slip velocity was found to be considerably decreased with increasing concentration and therefore the intrinsic convection to be diminished.¹⁰

It is the purpose of the present paper to examine whether intrinsic convection can be seen experimentally and, if it exists, how its amplitude varies with particle concentration. To this end, we have developed an experimental system to measure the particle sedimentation velocity across the width of the sedimentation cell. This system is derived from that used by Nicolai *et al.*¹¹ where marked particles are tracked in a sedimenting suspension of unmarked spheres made optically transparent by matching the index of refraction of the fluid to that of the glass spheres. If intrinsic convection exists, the particles should settle faster in the center of the cell than near the side walls. Indeed, this difference should be due to the global convection of the suspension which is superimposed on the settling motion of the particles relative to the suspension, this latter being independent of the shape of the cell.

In addition to measurement of the variation of the mean velocity, this experimental technique also provides the varia-

tion of the velocity fluctuations across the width of the cell. No prediction concerning these velocity fluctuations has been given by theories of intrinsic convection. However, these fluctuations have been found to be of the order of the mean and to have a diffusive long time behavior, known as hydrodynamic self-diffusion, in experiments^{11–13} performed in the whole cell, i.e., in different regions of the suspension across the cell. These fluctuations were shown to be independent of the size of the settling vessel.¹⁴

Since the variation of the particle concentration across the cell width is of fundamental importance for the origin of the intrinsic convection, as has been emphasized by the boundary layer approach,⁸ we have also performed light attenuation measurements through the suspension across the cell. These measurements, as well as visualization of the suspension, provide information regarding the particle concentration variation near the wall.

The present paper is organized as follows. The experimental techniques are presented in Sec. II. The experimental results are described and compared with theoretical predictions in Sec. III and then discussed in Sec. IV.

II. EXPERIMENTAL TECHNIQUES

A. Particles and fluid

The particles were glass beads with index of refraction 1.5190 ± 0.0002 , density $\rho_p = 2.53 \pm 0.02 \text{ g/cm}^3$ and radius $a = 394 \pm 17 \text{ }\mu\text{m}$. This batch of spheres was the same as that used by Nicolai *et al.*¹¹ and was supplied by the Laboratoire Central des Ponts et Chaussées. A fraction of these particles was uniformly silvered so that they could be tracked in the midst of an optically transparent sedimenting suspension of like particles. The thin coating of silver did not modify the particle settling characteristics.

The suspending fluid was an alkyl benzyl phthalate plasticizer named Santicizer 278 and produced by Monsanto. The matching of the refractive index of the fluid with that of the glass beads of the suspension was ensured by air-conditioning the laboratory room at $22 \pm 1 \text{ }^\circ\text{C}$. At this temperature, the fluid viscosity was $\eta = 13 \pm 2 \text{ P}$ and the fluid density was $\rho_f = 1.09 \pm 0.01 \text{ g/cm}^3$.

For this combination of fluid and spheres, the Stokes' velocity of an isolated sphere, $V_S = 2(\rho_p - \rho_f)a^2g/9\eta$ (g is the acceleration due to gravity), was $0.038 \pm 0.006 \text{ cm/s}$ (the error bar is mainly due to particle size dispersion), the sphere Reynolds number, $aV_S\rho/\eta$, was smaller than 10^{-3} and the Brownian Péclet number, aV_S/D_B , was very large (D_B is the Brownian diffusivity of the spheres).

B. Particle tracking

Experiments were performed in two glass walled cells (1 and 2). Cell 1 had a rectangular cross section with an inside width $b = 10.00 \pm 0.05 \text{ cm}$, an inside depth of $4.00 \pm 0.05 \text{ cm}$, and a height of $50.00 \pm 0.05 \text{ cm}$. Cell 2 had an inside square cross section of $4.00 \pm 0.05 \text{ cm}$ by $4.00 \pm 0.05 \text{ cm}$ ($b = 4.00 \pm 0.05$) and a height of $50.00 \pm 0.05 \text{ cm}$. Experiments were carried out by introducing weighted amounts of fluid and silvered and unsilvered spheres into the cell until the desired particle volume fraction was reached.

Typically, about 0.05% of the beads were silvered particles. A single particle volume fraction of 20% was studied with cell 1. Five particle volume fractions (5%, 10%, 20%, 30%, and 40%) were studied with cell 2. The experimental relative error in particle volume fraction measurements was about 4%.

During the experiments, the cell was held in a fixed position on a rail and the cell walls were oriented vertically within 0.05 cm. The cell was uniformly lit from behind and the silvered particles were then easily tracked with a charged coupled device camera (512×512 pixels) connected to a real time digital imaging system. The camera was focused in the median plane of the cell (midway between the front and the back walls). The depth of field of the imaging system corresponded to the depth of the cell ($= 4 \text{ cm}$). The camera recorded trajectories of silvered spheres settling in a square window of approximately $4 \times 4 \text{ cm}$ located in the middle region of the cell far from the sedimentation front and the sediment growth. This window captured the full width of cell 2. However, it was not wide enough to comprise the full width of the cell 1. In this case, two sets of experiments were undertaken. The window was located in the left half-width of the cell for the first set of experiments and in the right half-width of the cell for the second. An overlap between the two locations of the window provided measurement continuity. The size of the silvered particles corresponded to at least 9 pixels. In order to reduce the experimental error in the measurement of the instantaneous velocity for $\phi \geq 30\%$ with cell 2, a larger magnification was used which made the silvered particles approximately 17 pixels. Indeed, the experimental error in the measurement of the local particle velocity can become large for high volume fractions with a small image magnification since the particle displacement can be about the uncertainty in the measurement of the particle center of mass during the sampling time (see Nicolai *et al.*¹¹ for further discussion regarding sampling problems). In this latter case, the window, which could not again comprise the full width of the cell, was located in an half-width of cell 2.

The experimental procedure was identical for each experiment. It consisted of carefully mixing the suspension, allowing the suspension to settle for a short time and then tracking the silvered particles as soon as they entered the imaging window. The suspension was mixed with a small propeller fixed to the end of a shaft driven by a variable-speed drill motor. The propeller was moved randomly within the suspension in order to obtain a uniform particle distribution throughout the suspension. We checked the homogeneity of the mixing by examining the attenuation of a laser beam through the suspension (see the principle of the light attenuation technique described in Sec. II C). The mixing was stopped when the light attenuation reached a constant value in a given location as well as across different locations in the suspension. After the cessation of mixing, a short time of approximately 1 min was necessary for the upper front between the suspension and the clear fluid to form and then particle tracking began. The experiment was terminated when the upper front arrived 7 cm above the imaging window. This yielded a recording time during an experiment of 5–20 min depending upon the volume fraction.

Additional experiments were performed to examine the variation of the settling of a single silvered sphere across the cell containing only the fluid. The sphere was positioned in the top of the median plane of the cell but at a given location from the side of the cell. The sphere was then allowed to settle and particle tracking was started as soon as the sphere reached the top of the window. The experiment ended when the sphere reached the bottom of the window. Different experiments corresponding to different starting locations were performed.

To check whether a convection current existed in the cell containing only the fluid, the trajectory of a nearly buoyant particle was also examined. A small convection current due to a small thermal gradient was found across the cell. It was however of the order of 10^{-4} cm/s which is significantly less than the error in particle velocity measurements (see Sec. III A).

The imaging system consisted of the video camera connected to a fast and intelligent image processing and acquisition board (Matrox Image 1280), located in a personal computer operating with a digital imaging software package (Visilog 4.1 by Noesis). The tracking was achieved in real time with a specially designed program which allowed the localization of the center of mass of the projection of the silvered particle onto the window plane. The horizontal and vertical coordinates of the projected center of mass were recorded as a function of time into a file. The experimental error in the particle center measurement was of the order of one pixel. It should be mentioned that the major part of this error comes from the image threshold because of small imperfections in the homogeneity of the cell illumination. On the other hand, the resolution of the center of mass is very precise (~ 0.1 pixels). The sampling time, that is the time between two particle center recordings, had an average value of 2 s. It should be mentioned that this sampling time was always smaller than the time a test particle takes to traverse the recording window (between 2 min and 7 min depending upon the particle volume fraction). Typically 1000 particle trajectories were recorded for each volume fraction. However, since the objective of the experiments was to study the variation of particle velocity across the width of the cell, we only selected particles located in the middle depth of the cell. We visually chose particles located between the middle depth plane and a plane located at 5 mm from the inner front wall of the cell. After this selection, approximately 500 particle trajectories remained, which provide a statistically satisfactory data ensemble.

Except for some slight modifications, this tracking technique replicated that used by Nicolai *et al.*¹¹ where further details of the experimental technique and statistical analyses may be found.

C. Light attenuation measurements

In order to examine the variation of the particle concentration across the cell, measurements of the attenuation of light through the suspension across the cell were performed with the imaging system. The basic principle behind this light attenuation technique is that the amount of light attenuation by particles in a suspension is a function of the particle

concentration (see for instance the use of this technique in the case of fluidized beds^{15,16} and in the case of sedimenting suspensions¹⁷).

The experimental set up was identical to that described in the preceding Sec. II B. The light attenuation measurements were only performed in cell 2 for the five particle volume fractions (5%, 10%, 20%, 30%, and 40%). The cell was again uniformly lit from behind. The suspension was carefully mixed and was allowed to settle for a short time (the same as that used for the particle tracking). The video output of the camera was set to be linearly proportional to the received light quantity. A horizontal line of 512 pixels corresponding to the full width of the cell (or part of its width) was sampled 1000 times during the same recording time that was used for particle tracking and then averaged. The line was chosen to be located in the middle region of the cell far from the sedimentation front and the sediment growth. This measurement provided the gray level intensity of the light, I , transmitted through the suspension across the cell. The same measurement was performed through the pure fluid and yielded the light intensity, I_0 , across the cell for zero particle volume fraction. The attenuation of the light was then defined by I/I_0 . Since the index of the suspending fluid was matched with that of the particles, this light attenuation was mainly due to light scattering by the surfaces of the spheres.

D. Visualization of the sedimenting suspension

In order to examine the structure of the suspension, magnified pictures of the sedimenting suspension near the wall were also recorded with the camera. The depth of field was about 1 cm. Because of the index matching, the bulk of the particles was nearly transparent. Conversely, the rim of the projected particles could be clearly observed, therefore providing information about the suspension microstructure near the wall.

III. EXPERIMENTAL RESULTS

A. Statistical analysis of particle trajectories

Typical particle trajectories are presented in the 4×4 cm window containing the full cell width for cell 2 at $\phi = 20\%$ in Fig. 1. The trajectories are rather tortuous and present many loops as previously noted by Nicolai *et al.*¹¹ Since one of the objectives of this work was to measure the variation of the mean velocity and the velocity fluctuations across the cell width, this recording window was divided in 4 mm wide (~ 10 particle radius wide) vertical slices as indicated in Fig. 1 and therefore the square section cell width was divided into 10 slices. At the large concentrations for which a larger magnification was used, the window corresponding to half of the square cell was divided into 5 slices. In the case of the rectangular section cell 1, the recording window which contains only half of the cell width was divided in 5 mm wide (~ 12 particle radius wide) vertical slices and therefore, after combining the results of two half-width windows, the full width of the cell was finally divided into 20 slices.

Horizontal and vertical instantaneous velocities of a particle were calculated over each sampling time. Mean and

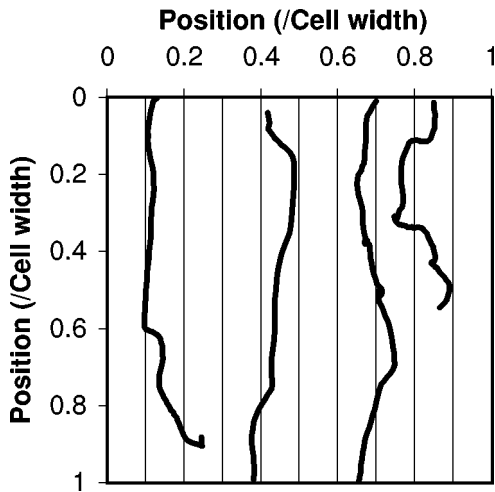


FIG. 1. Typical particle trajectories for cell 2 at $\phi=20\%$. The coordinates are normalized by the cell width, b .

standard deviation, $\langle V_p \rangle(x)$ and $\sigma_{V_p}(x)$, respectively, of the instantaneous velocities for all times and all tracked particles located in the slice x were then determined. Here and in the remainder of the paper, the brackets $\langle \rangle$ mean ensemble average. Typically, for each slice, the number of instantaneous velocities was of the order of 5000 for the rectangular cell 1 and 3000 for the square cell 2. We also computed the mean and standard deviation, $\langle V_p \rangle$ and σ_{V_p} , respectively, of the instantaneous velocities for all times and all tracked particles across the entire cell width. We checked that the histograms of the velocities, in each slice as well as in the whole cell width, were all found to be very smooth and approximately Gaussian, and therefore well represented by the mean and standard deviation.

The experimental errors in the mean and standard deviation were also estimated by computing the usual propagation of errors in simple measurements, such as the particle coordinates and sampling time. We also computed the statistical error in the mean, i.e., the 68% confidence limit, as the standard deviation divided by the square root of the number of uncorrelated instantaneous velocities. We assumed that the local velocities remain correlated only during the time for the velocity autocorrelation function to drop to the noise level. This time was chosen to be that found by Nicolai *et al.*¹¹ ($\sim 60a/V_S$) for all volume fractions in experiments performed in the whole cell. Since the statistical errors in the mean were always found to be larger than the experimental errors in the mean, they were considered the more representative.

B. Influence of the shape of the cell on particle velocity

The variations of the mean horizontal and vertical particle velocities, $\langle V_{p\perp} \rangle(x)$ and $\langle V_{p\parallel} \rangle(x)$, respectively, with the horizontal position x (measured from the left inside side of the cell) are displayed in Fig. 2(a) for the rectangular cell 1 at $\phi=20\%$. The velocities have been normalized by the mean settling velocity, $\langle V_{p\parallel} \rangle$, for all instantaneous vertical velocities across the entire cell width. The horizontal posi-

tion x has been normalized by the width of the cell ($=b=10.00\pm 0.05$ cm). The horizontal positions, x , of the experimental data correspond to the centers of the slices. Clearly, the mean vertical particle velocity varies across the cell. The particles settle faster in the center of the cell than near the side walls. This finding demonstrates the existence of a global intrinsic convection in the cell. The measured mean horizontal velocities are zero within error bars across the cell width.

In Fig. 2(a), the experimental results are also compared with the theoretical predictions for the same three-dimensional rectangular section cell in the case of dilute suspensions (without hydrodynamic interactions). The theoretical computation is derived from the classical expression for a Poiseuille flow in a three-dimensional rectangular section cell with a slip velocity at the wall, $w_* = 9V_S\phi/4$.¹⁰ It provides the variation of the suspension velocity, i.e., the velocity of the mixture of the particles and fluid, across the cell. To obtain the variation of the particle settling velocity, the particle velocity relative to the suspension velocity, which is shape independent and is equal to $\langle V_{p\parallel} \rangle$ (average over the whole cell width), must be added to this suspension velocity. The vertical velocity in the center of the measurement zone (a plane located 12.5 mm from the inner front wall of the cell) and the more realistic velocity averaged over the measurement zone (between the middle depth plane and a plane located at 5 mm from the inner front wall of the cell) have been computed. There is so little difference between these two theoretical velocities that the two curves cannot be distinguished.¹⁰ The shape of the theoretical flow is in qualitative agreement with the experimental data. However, the amplitude of the experimental intrinsic convection is much smaller than that predicted. It corresponds to 12% of the theoretical prediction.

The variations of the horizontal and vertical particle velocity fluctuations, $\sigma_{V_{p\perp}}(x)$ and $\sigma_{V_{p\parallel}}(x)$, respectively, normalized by $\langle V_{p\parallel} \rangle$, with the horizontal position x/b are presented in Fig. 2(b) for the rectangular cell 1 at $\phi=20\%$. Both fluctuations seem approximately constant in the center of the cell and present a decrease near the side walls. The relative vertical particle velocity fluctuations, $\sigma_{V_{p\parallel}}(x)/\langle V_{p\parallel} \rangle \times(x)$, do not seem to vary significantly across the cell [see Fig. 2(c)]. The fluctuation anisotropy, $\sigma_{V_{p\parallel}}(x)/\sigma_{V_{p\perp}}(x)$, is approximately constant in the center of the cell and increases near the side walls [see Fig. 2(d)].

It is interesting to notice that the experimental mean velocities and velocity fluctuations over the entire cell width (see Table I) are in good agreement with those measured by Nicolai *et al.*¹¹ in the middle width of the same rectangular cell but over the cell depth at the same volume fraction and for the same fluid and particles (see their Table I). This indicates the perfect reproducibility of the experiments. It also confirms that by averaging local velocities over the width or over the depth of the cell, i.e., by averaging out the intrinsic convection, one indeed obtains the mean particle velocity relative to the suspension. It should be mentioned that, to obtain the correct measurement of the mean particle velocity relative to the suspension, one would need to average over

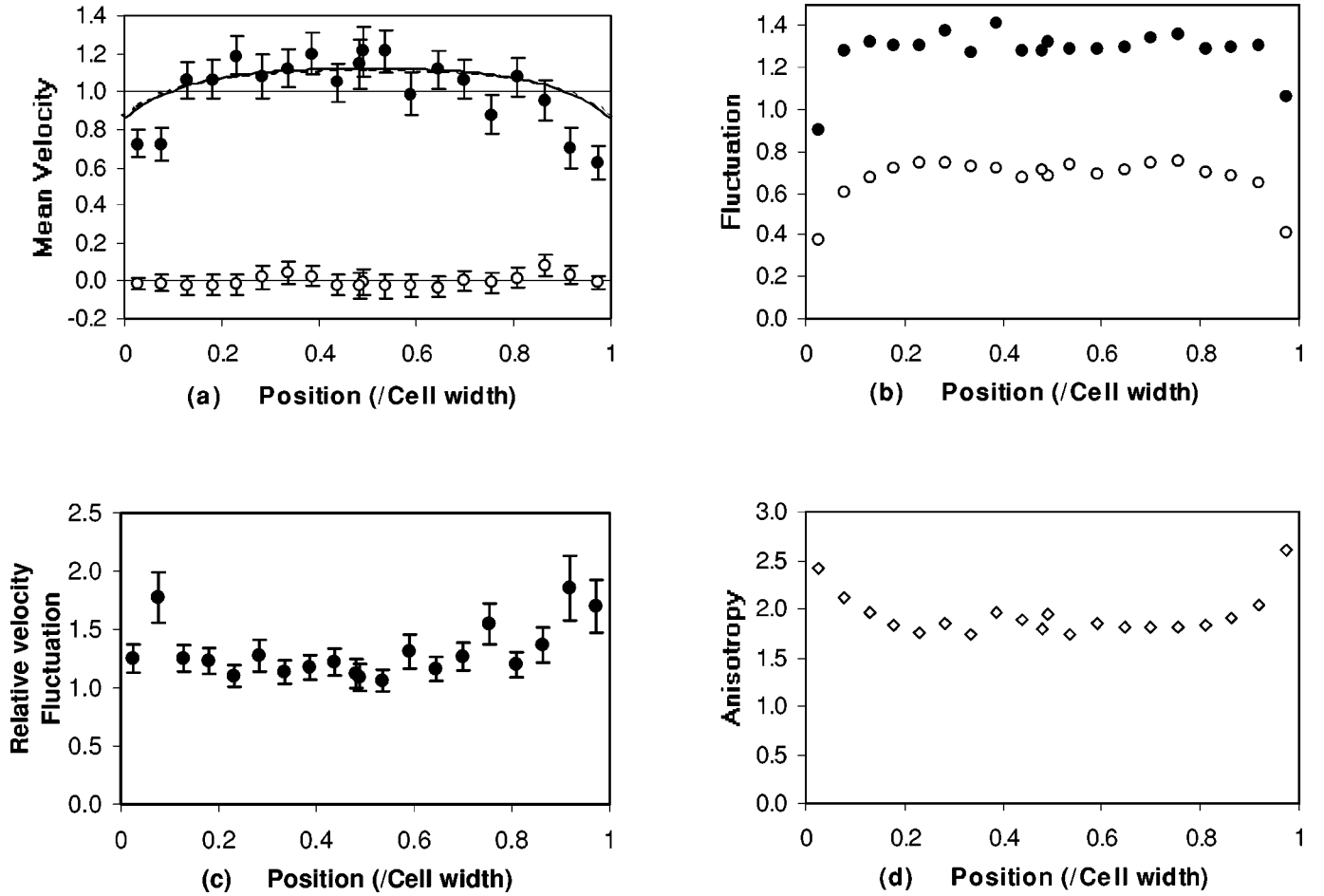


FIG. 2. Results versus x/b for cell 1 at $\phi=20\%$: (a) Normalized mean horizontal and vertical particle velocities, $\langle V_{p\perp}(x) \rangle / \langle V_{p\parallel} \rangle$ (\circ) and $\langle V_{p\parallel}(x) \rangle / \langle V_{p\parallel} \rangle$ (\bullet), respectively (the solid curve is the theoretical vertical velocity in the center of the measurement zone and the dashed curve is the theoretical vertical velocity averaged over the measurement zone with the amplitude of the intrinsic convection fixed at 12% of the theoretical prediction). (b) Normalized horizontal and vertical particle velocity fluctuations, $\sigma_{V_{p\perp}}(x) / \langle V_{p\parallel} \rangle$ (\circ) and $\sigma_{V_{p\parallel}}(x) / \langle V_{p\parallel} \rangle$ (\bullet), respectively. (c) Relative vertical particle velocity fluctuations, $\sigma_{V_{p\parallel}}(x) / \langle V_{p\parallel}(x) \rangle$ (\bullet). (d) Particle velocity fluctuation anisotropy, $\sigma_{V_{p\parallel}}(x) / \sigma_{V_{p\perp}}(x)$ (\diamond).

the entire cell and not over the width or the depth individually. However, there is only few percent difference between averaging over the entire cell and over the width (or the depth). In any case, this difference is smaller than the error bars.

C. Influence of particle concentration on particle velocity

The variation of the amplitude of the intrinsic convection with particle volume fraction was examined in cell 2. Although intrinsic convection is predicted theoretically to arise for dilute suspensions,^{3,8,10} no significant variation of the mean vertical particle velocity is measured across the cell for $\phi=5\%$, as displayed in Fig. 3(a). At larger volume fractions ($\phi=10\%$ and 20%), the particles settle faster in the center

of the cell than near the side walls as shown in Figs. 3(b) and 3(c). However, the amplitude of the experimental intrinsic convection is much smaller than the predictions of the dilute theories.^{3,8,10} Moreover, the experimental convection is smaller at $\phi=20\%$ than at $\phi=10\%$. As the concentration is further increased ($\phi=30\%$), the mean vertical velocity near the wall seems slightly larger than the velocities in the center as shown by the results of two different sets of experiments in Fig. 3(d). This finding suggests that there is an intrinsic convection in the opposite direction. However, the amplitude of this inverse convection is very small and at the limit of the present experimental resolution. At even larger volume fraction ($\phi=40\%$), no notable variation is measured across the cell. The measured mean horizontal velocities are zero within error bars across the cell width for all volume fractions.

The amplitude of the intrinsic convection is plotted as a function of particle volume fraction, ϕ , in Fig. 4. There are different ways to define this amplitude. We chose to define it as $(\langle V_{p\parallel} \rangle_m - \langle V_{p\parallel} \rangle) / V_S$ where $\langle V_{p\parallel} \rangle_m$ is the mean vertical velocity of particles located in the middle 40% of the cell width. The advantage of this definition is that $\langle V_{p\parallel} \rangle_m$ and $\langle V_{p\parallel} \rangle$ are measured very accurately. Other definitions such as

TABLE I. Mean velocities and velocity fluctuations over the whole width of cell 1. The results are made dimensionless by scaling with the theoretical value of the Stokes' velocity, V_S .

ϕ	$\langle V_{p\perp} \rangle / V_S$	$\langle V_{p\parallel} \rangle / V_S$	$\sigma_{V_{p\perp}} / V_S$	$\sigma_{V_{p\parallel}} / V_S$
0.200 ± 0.008	0.000 ± 0.005	0.39 ± 0.06	0.26 ± 0.05	0.50 ± 0.08

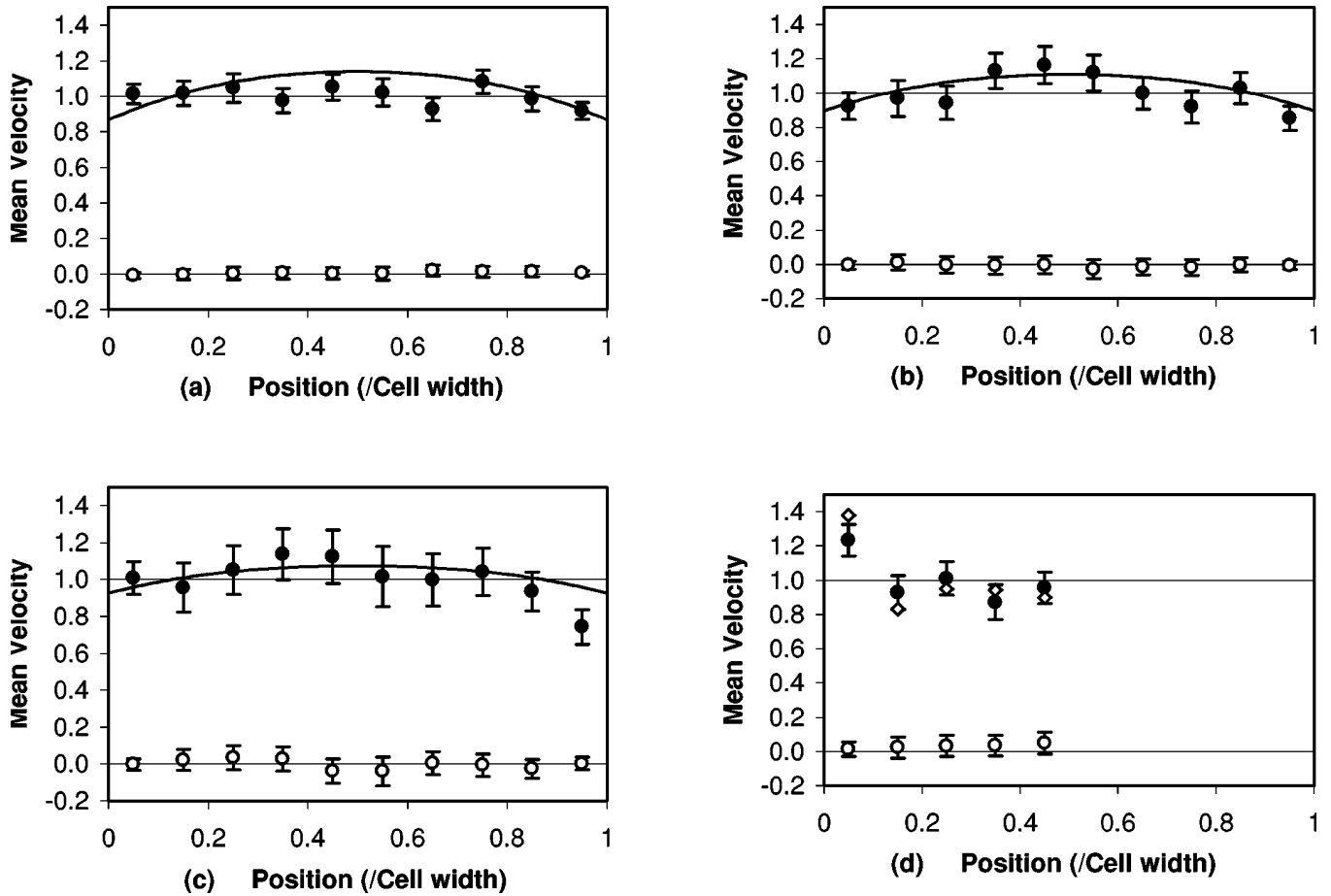


FIG. 3. Normalized mean horizontal and vertical particle velocities, $\langle V_{p\perp} \rangle(x)/\langle V_{p\parallel} \rangle$ (\circ) and $\langle V_{p\parallel} \rangle(x)/\langle V_{p\parallel} \rangle$ (\bullet), respectively, versus x/b for cell 2 at (a) $\phi=5\%$ (the solid curve is the theoretical vertical velocity in the center of the measurement zone with the amplitude of the intrinsic convection fixed at 100% of the theoretical prediction), (b) $\phi=10\%$ (the solid curve is the theoretical vertical velocity in the center of the measurement zone with the amplitude of the intrinsic convection fixed at 35% of the theoretical prediction), (c) $\phi=20\%$ (the solid curve is the theoretical vertical velocity in the center of the measurement zone with the amplitude of the intrinsic convection fixed at 7% of the theoretical prediction), and (d) $\phi=30\%$ [a second set of data for the vertical velocity is also presented (\diamond)].

the difference between velocities in the middle of the cell and near the wall, give similar variation as a function of concentration. However, since the settling velocity near the wall is affected by particle-walls interaction, it is better to

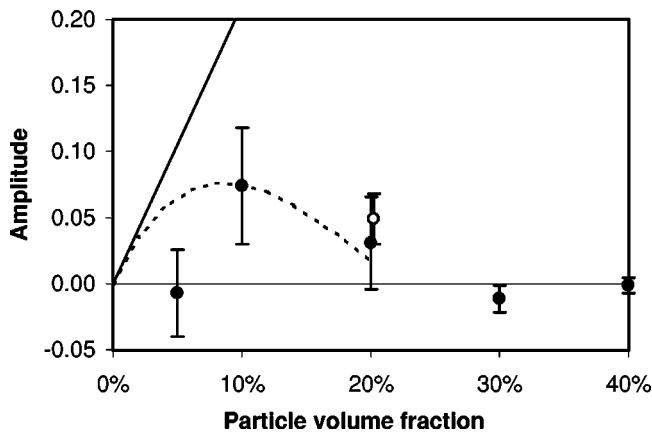


FIG. 4. Amplitude of the intrinsic convection, $(\langle V_{p\parallel} \rangle_m - \langle V_{p\parallel} \rangle)/V_S$, versus ϕ for cell 1 (\bullet) and cell 2 (\circ). The solid straight line is the theoretical prediction of the three-dimensional dilute theory. The dashed curve is the theoretical prediction of the model which assumes a Percus-Yevick approximation for the distribution of spheres.

use the settling velocity in the middle to determine the global convection motion. This amplitude is zero at small volume fraction $\phi=5\%$, attains a maximum value at about $\phi=10\%$, decreases for larger volume fraction to become slightly negative at $\phi=30\%$, and then is zero for $\phi>30\%$. It is interesting to notice that the amplitude of the intrinsic convection is approximately the same for the two cells at $\phi=20\%$. The dilute theory predicts that the amplitude is slightly larger for a squared section cell (the shape of the flow is somehow flatter in the center for a rectangular section cell).¹⁰ However, because of the data scatter, such a subtle difference cannot be measured experimentally. In Fig. 4, the experimental results are also compared with the predictions of the three-dimensional theory.¹⁰ Same definition has been adopted for the amplitude of the intrinsic convection. In particular, $\langle V_{p\parallel} \rangle_m$ has been averaged in the same middle 40% of the flow. The velocity difference is then simply $\langle V_{p\parallel} \rangle_m - \langle V_{p\parallel} \rangle = 0.94w_*$ where $w_* = 9V_s\phi/4$ in the dilute theory and w_* is given in Fig. 4 of Bruneau *et al.*¹⁰ when concentration effects are included by assuming a Percus-Yevick distribution of spheres near the walls. Clearly, the results of the experiments disagree with those of the dilute theory which predicts a linear variation with volume fraction.

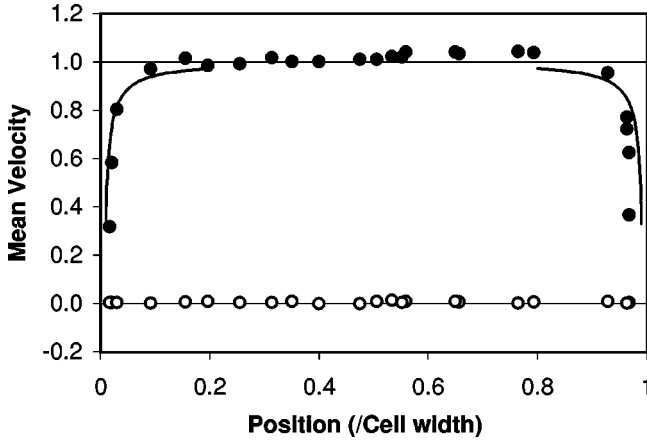


FIG. 5. Normalized mean horizontal (\circ) and vertical velocities (\bullet) of a single sphere versus x/b for cell 2 containing only the fluid. The results are made dimensionless by scaling with the theoretical value of the Stokes' velocity, V_S , of the sphere. The solid curve is the theoretical prediction for the vertical velocity near the wall.

When the effect of particle concentration is included, the agreement is better.

We have also plotted, for comparison, in Fig. 5 the variation of the settling velocity of a single sphere with the horizontal position x/b for cell 2 containing only the fluid. The experimental data are in perfect agreement with the theoretical results of the Stokes' equation.^{18–21} The measured settling velocity in the middle of the cell is found to be in good agreement with the theoretical value of the Stokes' velocity, V_S . The horizontal velocity is zero within error bars. We can see that, unlike the intrinsic convection which has an effect up to the middle of the cell, the influence of the wall extends only about 10 particle radii for a single particle.

Plots of normalized horizontal and vertical particle velocity fluctuations, $\sigma_{V_{p\perp}}(x)/\sigma_{V_{p\perp}}$ and $\sigma_{V_{p\parallel}}(x)/\sigma_{V_{p\parallel}}$, versus x/b are presented in Fig. 6 for different ϕ . As a general trend, both fluctuations seem approximately constant in the center of the cell and present a decrease near the side walls

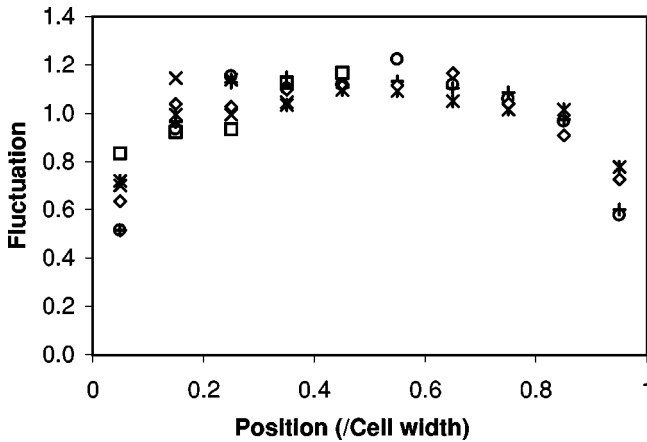


FIG. 6. Normalized horizontal and vertical particle velocity fluctuations, $\sigma_{V_{p\perp}}(x)/\sigma_{V_{p\perp}}$ and $\sigma_{V_{p\parallel}}(x)/\sigma_{V_{p\parallel}}$, respectively, versus x/b for cell 2 at (a) $\phi=5\%$ (\circ and $*$, respectively), (b) $\phi=20\%$ (\diamond and $+$, respectively), and (c) $\phi=40\%$ (\square and \times , respectively).

TABLE II. Mean velocities and velocity fluctuations over the whole width of cell 2 (or over half the width of cell 2 for $\phi \geq 30\%$). The results are made dimensionless by scaling with the theoretical value of the Stokes' velocity, V_S .

ϕ	$\langle V_{p\perp} \rangle / V_S$	$\langle V_{p\parallel} \rangle / V_S$	$\sigma_{V_{p\perp}} / V_S$	$\sigma_{V_{p\parallel}} / V_S$
0.050 ± 0.002	0.005 ± 0.008	0.8 ± 0.1	0.25 ± 0.04	0.54 ± 0.09
0.100 ± 0.004	-0.01 ± 0.01	0.7 ± 0.1	0.31 ± 0.05	0.6 ± 0.1
0.200 ± 0.008	-0.001 ± 0.008	0.43 ± 0.07	0.25 ± 0.04	0.52 ± 0.09
0.30 ± 0.01^a	0.004 ± 0.004	0.13 ± 0.02	0.10 ± 0.02	0.14 ± 0.02
0.30 ± 0.01^b	-0.002 ± 0.005	0.11 ± 0.02	0.11 ± 0.02	0.15 ± 0.03
0.40 ± 0.02	0.001 ± 0.002	0.06 ± 0.01	0.031 ± 0.005	0.05 ± 0.01

^aFirst set of experiments.

^bSecond set of experiments.

as previously noted in Fig. 2. This behavior is observed even in the absence of measured intrinsic convection.

It is important to mention that the experimental mean velocities and velocity fluctuations over the entire width of cell 2 (see Table II) are of the same order of magnitude as those measured by Nicolai *et al.*¹¹ over the entire depth of cell 1 and for the same fluid and particles (see their Table I). This confirms that velocity fluctuations do not vary with the size of the cell.¹⁴ It should be noted that the velocity fluctuation computed over the entire cell are also of the same order of magnitude as those measured by Xue *et al.*¹³ However the decrease of the relative velocity fluctuations above $\phi=30\%$ in these later experiments performed in a fluidized bed is, however, stronger than in the present results and those of Nicolai *et al.*¹¹

D. Structure of the suspension near the wall

Plots of the light attenuation, I/I_0 , versus $x/2a$ (measured from the left inside side of the cell) are presented for the different volume fractions in Fig. 7. For all volume fractions, the attenuation is approximately constant except near the wall. The noise in the data results from statistical fluctuations in the number and the position of the particles. For $\phi \geq 5\%$, there is a larger transmission very close to the wall but there exists a decrease at about one particle diameter. At $\phi=30\%$, the attenuation exhibits an additional oscillation. For larger volume fraction ($\phi=40\%$), the attenuation is so strong that it is very difficult to detect its small variations. It should be also mentioned that these attenuation measurements are very reproducible for each concentration. The constant attenuation in the uniform middle region of the cell is plotted as a function of the particle volume fraction in Fig. 8. It is a monotonically decreasing function which was used to calibrate the light attenuation, I/I_0 . The logarithm of I/I_0 can indeed be fitted to a linear function of ϕ by using a linear regression. The best fit is found to be $\ln(I/I_0) = -8.1\phi$. We can then determine the variation of the local volume fraction $\phi(x)$ across the cell. The difference $\phi(x) - \phi$ versus $x/2a$ is displayed in Fig. 9. There is clearly a deficit of particles near the wall but there exists an accumulation of particles at about a diameter from the wall. There is a second accumulation zone at about 1.8 diameter for $\phi=30\%$. The oscillating behavior of particle volume fraction near the wall is similar but quantitatively different to that deduced from a Percus-Yevick

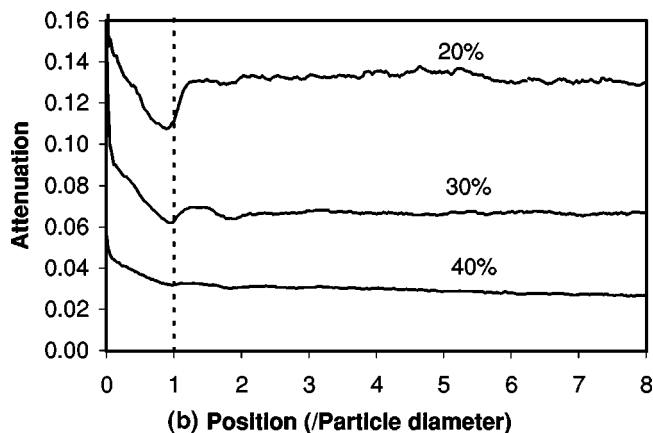
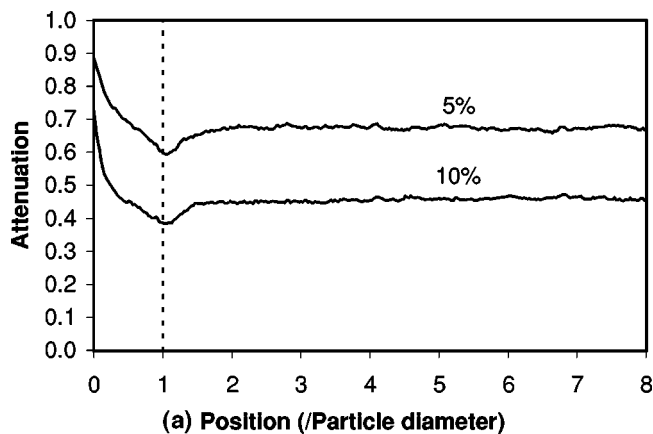


FIG. 7. Plots of the light attenuation, I/I_0 , versus $x/2a$ for (a) $\phi=5\%$ and 10% and (b) $\phi=20\%$, 30% , and 40% .

equilibrium distribution function (see Fig. 3 of Bruneau *et al.*¹⁰). Indeed, peak positions are well predicted by the Percus-Yevick model but peak amplitudes are not. The amplitude of the first accumulation peak does not seem to vary with concentration while the model predicts an increase with concentration.

Visualization of the suspension microstructure confirms that there is particle ordering near the wall. In particular, there exists a layer of particles that pile up against the wall. This concentrated layer inside the suspension is clearly ob-

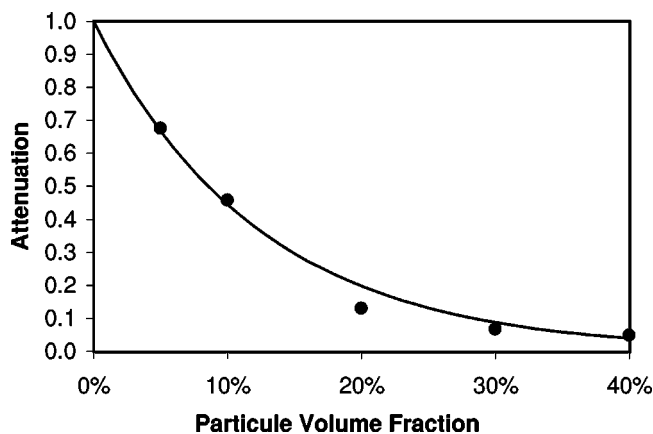


FIG. 8. Calibration of the attenuation, I/I_0 , with ϕ . Experimental data (●) and best fit (solid curve).

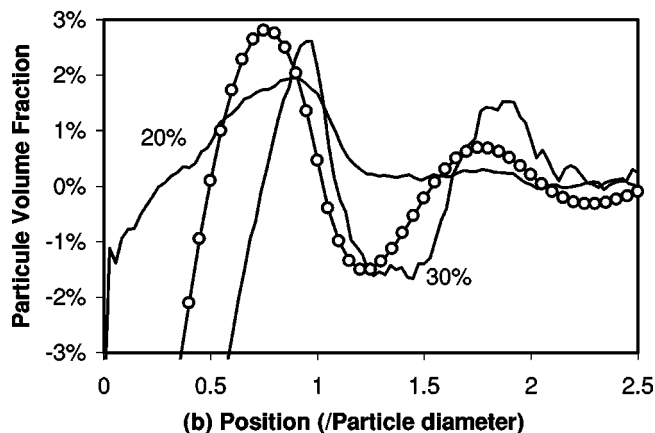
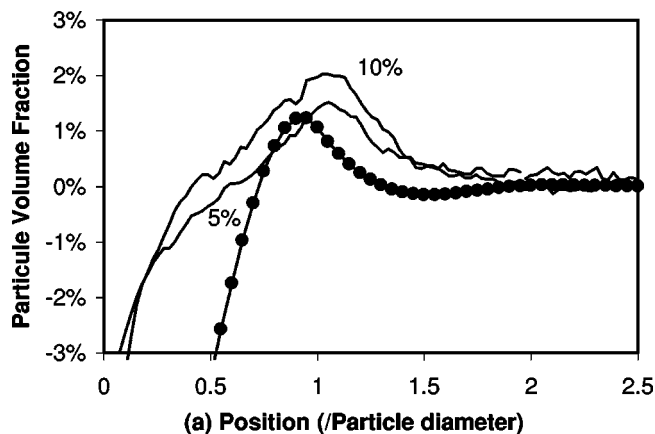


FIG. 9. Plots of the difference in particle volume fraction, $\phi(x) - \phi$, versus $x/2a$ (a) for $\phi=5\%$ and 10% (b) for 20% and 30% . The theoretical curves for $\phi=10\%$ (●) with the amplitude at 100% of the theoretical prediction and for $\phi=30\%$ (○) with the amplitude at 33% of the theoretical prediction are also provided. The experimental error in position is 0.1 diameter.

served at $\phi \geq 10\%$ (see Fig. 10). Moreover at $\phi=10\%$ and 20% , where intrinsic convection is observed, a layer of particles is left behind the sedimenting front between the clear fluid and the suspension as can be seen in Fig. 10 against the left lateral wall. We discovered that this latter layer is however very dilute by recording side pictures of the sedimenting front. This dilute layer (consisting of only few particles) can be also seen against the front wall behind the sedimenting front in Fig. 10.

We have estimated the velocity of the near wall concentrated layer inside the suspension from particle tracking experiments. The mean settling velocity of particles whose centers are located at about 1-2 radii from the wall, $\langle V_{p\parallel} \rangle_w$, are plotted as a function of ϕ in Fig. 11. For comparison, the decrease of the mean vertical velocity (average over the whole cell width, see Tables I and II), $\langle V_{p\parallel} \rangle$, with ϕ is also provided in Fig. 11. The velocities are made dimensionless by the Stokes' velocity. It should be mentioned that an important part of the error in dimensionless velocities comes from the error in Stokes' velocity (the uncertainty is mainly due to particle size dispersion). At volume fractions for which intrinsic convection is clearly observed ($\phi=10\%$ and 20%), the layer velocity, $\langle V_{p\parallel} \rangle_w$, is smaller than $\langle V_{p\parallel} \rangle$. It is interesting to mention that, at these volume fractions, the velocity of this layer relative to the suspension,

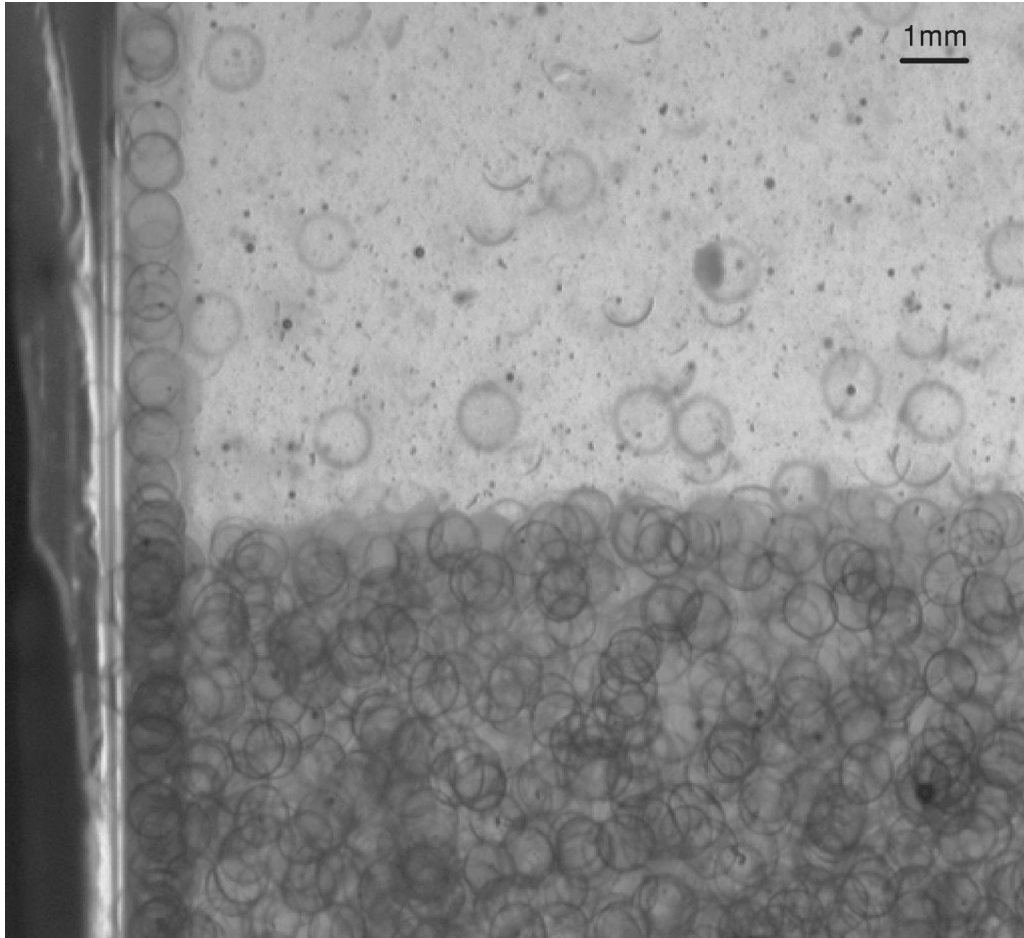


FIG. 10. Picture of the sedimenting suspension near the wall for cell 2 at $\phi=20\%$.

$\langle V_{p\parallel} \rangle_w - \langle V_{p\parallel} \rangle$, is much larger than the estimated slip velocity. At smaller ($\phi=5\%$) and larger ($\phi \geq 30\%$) volume fractions, the layer velocity, $\langle V_{p\parallel} \rangle_w$, is approximately equal to the settling velocity, $\langle V_{p\parallel} \rangle$.

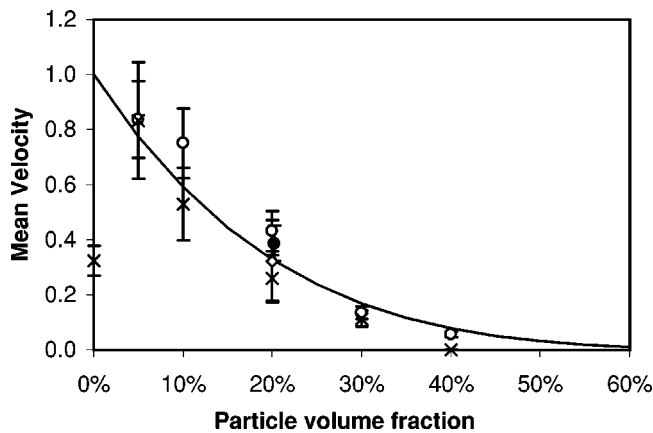


FIG. 11. Mean velocity over the whole cell width (● for cell 1 and ○ for cell 2), $\langle V_{p\parallel} \rangle$ and mean settling velocity of the particles located in the layer near the wall (◇ for cell 1 and × for cell 2), $\langle V_{p\parallel} \rangle_w$ (the datum at $\phi=0\%$ comes from that of Fig. 5 at the wall). The results are made dimensionless by scaling with the theoretical value of the Stokes' velocity, V_S . The solid curve corresponds to the Richardson-Zaki law $(1-\phi)^5$ (Ref. 22).

IV. DISCUSSIONS AND CONCLUDING REMARKS

By measuring the mean particle settling velocity across the width of the sedimentation cell, we have shown that there can be a global intrinsic convection of the suspension superimposed on the settling motion of the particles. The amplitude of the intrinsic convection is found as a function of particle volume fraction. No convection is measured at low volume fraction ($\phi=5\%$). Conversely, at larger volume fraction ($\phi=10\%$), the particles settle faster in the center of the cell than near the side walls. The amplitude of the convection diminishes as the concentration is further increased ($\phi=20\%$). There may even be a convection in the opposite direction at $\phi=30\%$. However, if this inverse convection exists, its amplitude is very small and is at the limit of the present experimental resolution. At an even larger volume fraction ($\phi=40\%$), no significant velocity variation is observed across the cell. Light attenuation measurements as well as visualization of the suspension show that there is ordering of the particles near the wall for non-dilute suspensions ($\phi \geq 5\%$). Such behavior has been observed for concentrated suspensions under shear.^{23–25} In the present experiment, there is clearly a concentrated layer of particles that pile up against the wall. This layer settles slower than the bulk at concentrations for which convection is clearly observed ($\phi=10\%$ and 20%).

The results of the present experiments disagree with those of the dilute intrinsic convection theories which predict a linear variation of the convection amplitude with particle volume fraction.^{3,8,10} When the effect of particle concentration is included in the dilute model by assuming an equilibrium Percus-Yevick distribution of spheres near the wall,¹⁰ better agreement with experiments is found. As assumed by this latter theory, some ordering of the suspension near the wall is observed experimentally. However, the oscillating behavior of particle volume fraction near the wall is similar but quantitatively different to that deduced from an equilibrium distribution function. The contributions resulting from the dilute and dense regions near the wall may compensate and produce the observed decrease in the magnitude of the convection at large concentrations. This may even induce the small inverse convection which seems observed at $\phi=30\%$. Therefore this particle ordering near the wall seems very important for explaining the observed magnitude of the convection. A more accurate theoretical evaluation of the effect of concentrations would require one to combine a detailed investigation of the dynamic particle-wall distribution with the calculation of hydrodynamic interactions in presence of the wall (in particular lubrication forces).

The present experiments also provide the variation of the velocity fluctuations across the cell width. As a general trend, both horizontal and vertical fluctuations are approximately constant in the center of the cell and decrease near the side walls. This behavior is observed whether or not intrinsic convection is present. Therefore, it does not seem to be tightly linked to the intrinsic convection phenomenon. Instead, the wall appears to affect the magnitude of the fluctuations.

Finally, to complete the discussion, we may ask whether shear induced migration of particles, i.e., migration induced by the intrinsic convection flow is possible.^{26,27} Scaling arguments^{28,29} show that the settling length, h , necessary for particles to diffuse across the cell width is $h/b \sim \langle V_{p\parallel} \rangle \times (b^2/D_s)/b \sim b^2/a^2$ with a shear induced diffusivity $D_s \sim \dot{\gamma} a^2$ and a shear rate $\dot{\gamma} \sim \langle V_{p\parallel} \rangle / b$. In the present experiment, this length would be about $10000 \times b$ for cell 2 (and about $62500 \times b$ for cell 1), which is much larger than the cell height and therefore than the settling height. The particle density distribution across the cell (estimated from light attenuation measurements as shown in Fig. 7) does not seem, indeed, to vary during the settling process.

In summary, this work presents the first experimental evidence of the intrinsic convection of a uniform sedimenting suspension. This global convection of the suspension is found to be small and even to disappear with increasing concentrations. This contradicts the theoretical studies of Mazur and co-workers²⁻⁴ and those, more recent, of Bruneau *et al.*⁸ who predicted an $O(V_S \phi)$ amplitude of the convection for dilute suspensions. Another important experimental finding is that there is an ordering of the suspension near the wall. This ordering may be responsible for the observed small magnitude of the convection and for its vanishing at large concentrations.

ACKNOWLEDGMENTS

We wish to thank F. Feuillebois and E. J. Hinch for their many helpful comments and suggestions during the development of this work as well as providing us with the theoretical curves of Figs. 2, 3, 5, and 9. We also acknowledge discussions with J. F. Brady and D. T. Leighton on the problem of shear induced migration and D. Lhuillier on the macroscopic approach of intrinsic convection. This work is part of the thesis of Y. Peysson sponsored by the Ministère de l'Éducation Nationale, de l'Enseignement Supérieur et de la Recherche. It was also undertaken under the auspices of the Groupement de Recherche du CNRS "Physique des Milieux Hétérogènes Complexes" and the European network "Co-operative Phenomena in Complex Systems." The Santicizer 278 was donated by Monsanto.

- ¹G. K. Batchelor, "Sedimentation in a dilute dispersion of spheres," *J. Fluid Mech.* **52**, 245 (1972).
- ²C. W. J. Beenakker and P. Mazur, "Is sedimentation container-shape dependent?," *Phys. Fluids* **28**, 3203 (1985).
- ³U. Geigenmüller and P. Mazur, "Sedimentation of homogeneous suspensions in finite vessels," *J. Stat. Phys.* **53**, 137 (1988).
- ⁴U. Geigenmüller and P. Mazur, "Intrinsic convection near a meniscus," *Physica A* **171**, 475 (1991).
- ⁵P. Nozière, "A local coupling between sedimentation and convection: Application to the Beenakker-Mazur effect," *Physica A* **147**, 219 (1987).
- ⁶B. Noetinger, "A two fluid model for sedimentation phenomena," *Physica A* **152**, 1139 (1989).
- ⁷P. Mazur and W. van Saarloos, "Many-sphere hydrodynamic interactions and mobilities in a suspension," *Physica A* **115**, 21 (1982).
- ⁸D. Bruneau, F. Feuillebois, R. Anthore, and E. J. Hinch, "Intrinsic convection in a settling suspension," *Phys. Fluids* **8**, 2236 (1996).
- ⁹J. Blawdziewicz and F. Feuillebois, "Calculation of an effective slip in a settling suspension at a vertical wall," *Fluid Mech. Res.* **22**, 81 (1996).
- ¹⁰D. Bruneau, F. Feuillebois, J. Blawdziewicz, and R. Anthore, "Three-dimensional intrinsic convection in dilute and dense dispersions of settling spheres," *Phys. Fluids* **10**, 55 (1998).
- ¹¹H. Nicolai, B. Herzhaft, E. J. Hinch, L. Oger, and E. Guazzelli, "Particle velocity fluctuations and hydrodynamic self-diffusion of sedimenting non-Brownian spheres," *Phys. Fluids* **7**, 12 (1995).
- ¹²J. M. Ham and G. M. Homsy, "Hindered settling and hydrodynamic dispersion in quiescent sedimenting suspension," *Int. J. Multiphase Flow* **14**, 533 (1988).
- ¹³J. Z. Xue, E. Helbolzheimer, M. A. Rutgers, W. B. Russel, and P. M. Chaikin, "Diffusion, dispersion and settling of hard spheres," *Phys. Rev. Lett.* **69**, 1715 (1992).
- ¹⁴H. Nicolai and E. Guazzelli, "Effect of the vessel size on the hydrodynamic diffusion of sedimenting spheres," *Phys. Fluids* **7**, 3 (1995).
- ¹⁵T. B. Anderson and R. Jackson, "A fluid mechanical description of fluidized beds—Comparison of theory and experiment," *Ind. Eng. Chem. Fundam.* **8**, 137 (1969).
- ¹⁶M. M. El-Kaissy and G. M. Homsy, "Instability waves and the origin of bubbles in fluidized beds. Part I. Experiments," *Int. J. Multiphase Flow* **2**, 379 (1976).
- ¹⁷R. H. Davis and K. H. Birdsell, "Hindered settling of semidilute monodisperse and polydisperse suspensions," *AIChE. J.* **34**, 123 (1988).
- ¹⁸W. R. Dean and M. E. O'Neill, "A slow rotation of viscous liquid caused by the rotation of a solid sphere," *Mathematika* **10**, 13 (1963).
- ¹⁹M. E. O'Neill, "A slow motion of viscous liquid caused by a slowly moving solid sphere," *Mathematika* **11**, 67 (1964).
- ²⁰M. E. O'Neill, "A slow motion of viscous liquid caused by a slowly moving solid sphere: An addendum," *Mathematika* **14**, 170 (1967).
- ²¹F. Feuillebois, "Some theoretical results for the motion of solid spherical particles in a viscous fluids," in *Multiphase Science and Technology*, edited by G. F. Hewitt, J. M. Delhay, and N. Zuber (Hemisphere, New York, 1989), p. 583.
- ²²J. F. Richardson and W. N. Zaki, "Sedimentation and fluidisation: Part I," *Trans. Inst. Chem. Eng.* **32**, 35 (1954).
- ²³I. Rampall, "Shear-induced structure and migration in non-colloidal suspensions," Ph.D. thesis, University of Notre Dame, 1992.

- ²⁴D. T. Leighton and I. Rampall, "Measurement of the shear-induced microstructure of concentrated suspensions of non-colloidal particles," in *Particulate Two-Phase Flow*, edited by M. C. Roco (Butterworth, Boston, 1993), p. 190.
- ²⁵G. P. Krishnan and D. T. Leighton, "Shear-induced structure in bidisperse suspensions," in *Program and Extended Abstracts of the IUTAM Symposium on Hydrodynamic Diffusion of Suspended Particles*, edited by R. H. Davis (University of Colorado, Boulder, 1995), p. 89.
- ²⁶D. Leighton and A. Acrivos, "The shear-induced migration of particles in concentrated suspensions," *J. Fluid Mech.* **181**, 415 (1987).
- ²⁷P. R. Nott and J. F. Brady, "Pressure-driven flow of suspensions: simulation and theory," *J. Fluid Mech.* **275**, 157 (1994).
- ²⁸J. F. Brady (private communication).
- ²⁹D. T. Leighton (private communication).